Supplementary Information (SI) for Journal of Materials Chemistry A.

Electronic Supplementary information for:

Ag_2O-Loaded Cu Based Metal-Organic Framework Material as Pre-Electrocatalyst for Efficient Urea Synthesis

Xinyao Quan,[1,a] Yulong Zhou,[1,a] Ruiling Du,[a,*] Lian Duan,[a] Gen Chen,[a] and Ning Zhang [a,*]

[1] These authors contribute equally to this work.

[a] School of Materials Science and Engineering, Central South University, Changsha, Hunan 410083, China.

* nzhang@csu.edu.cn; ruiling.du@csu.edu.cn

Content

Supplementary Figures

Figure S17. Long-term chronoamperometry tests for Cu BTC@Ag_2O.

Figure S18. Post-reaction analyses on the Cu BTC@Ag_2O catalyst.

Supplementary Tables

Table S1. Comparison of the electrocatalytic urea production of Cu BTC@Ag_2O catalyst with other extensively reported electrocatalysis.

Table S2. Adsorption configurations of $*CO_2$, *COOH, *CO on Ag, Cu, and Cu-Ag surfaces.

Table S3. Adsorption configurations of $*NO_3$, $*NO_2$, *NO, *N, *NH, $*NH_2$ on Ag, Cu, and Cu-Ag surfaces.

Table S4. Adsorption configuration of intermediates for C-N coupling on Ag, Cu, and Cu-Ag surfaces.

Experimental section

Materials. Potassium nitrate (KNO_3, AR, 99.5%), potassium nitrite (KNO_2, AR, 97%), potassium bicarbonate ($KHCO_3$, AR, 99.5%), benzene-1,3,5-tricarboxylic acid (BTC, AR, 99%), Copper nitrate trihydrate ($Cu\ (NO_3)_2 \cdot 3H_2O$, AR, 99%), silver nitrate ($AgNO_3$, AR, 99%) were purchased from Aladdin Industrial Corporation. Sulfuric acid (H_2SO_4, GR, 95~98%), hydrochloric acid (HCl, GR, 38%), sodium hydroxide (NaOH, AR, ⩾96%) were supplied by Sinopharm Chemical Reagent Co. Ltd. Diacetylmonoxime (DAMO, GC, 98.0 %), thiosemicarbazide (TSC, AR, 98.5%), sulfanilamide ($C_6H_8N_2O_2S$, AR, 99%), N-(1-Naphthyl) ethylenediamine dihydrochloride ($C_{12}H_{16}C_{12}N_2$, AR, 98%) were obtained from Shanghai Macklin Biochemical Co., Ltd. All reagents were used without further purification. Deionized water (DI, 18.2 MΩ) was used throughout the preparation of catalysts and the performance testing processes.

Characterization. The phases of catalysts were characterized using X-ray diffraction (XRD) (Rigaku Miniflex 600, Cu-Kα radiation with λ=1.51484Å) with a 2θ range from 5° to 80° and a scan rate of 4° min^{-1}. Scanning electron microscopy (SEM) images were obtained from a FEI Helios Nanolab 600 field emission electron microscope. FEI Tecnai G2 F20 field emission transmission electron microscopy (TEM) operated at 200 kV recorded TEM and HRTEM images. Energy-dispersive X-ray (EDX) elemental mapping was obtained with a TalosTM F200X field emission transmission electron microscope at 200 kV. X-ray photoelectron spectroscopy (XPS) spectra were measured by using a Thermo Fisher ESCALAB 250Xi spectrophotometer. The binding energy of 284.8 eV from the carbon 1s line is indeterminate carbon. UV−vis spectra were acquired with a UV-2600 spectrophotometer at room temperature. In situ electrochemical infrared (IR) measurements were conducted using a Thermo iS50 spectrometer. In situ electrochemical Raman spectra were collected using a Horiba Jobin-Yvon LabRAM HR800 with a 633 nm excitation laser. Modified H-type cell produced by Shanghai Chuxi Industrial Co., Ltd. was used in the Raman measurement. The working electrode, with a fixed area of 0.25 cm^2, was made of dry carbon fiber paper (CFP) modified with catalysts. Platinum foil and Ag/AgCl were used as the counter electrode and the reference electrode, respectively. CO_2 saturated 0.1 M $KHCO_3$ + 0.1 M KNO_3 mixed solution was used as electrolyte. The spectra depend on potentials were obtained by applying single potential steps and collected after running 30s. Thermogravimetric analysis (TGA) was performed using a NETZSCH STA 449 thermal analyzer (Germany) in an air atmosphere, with the temperature ramped from 25 °C to 800 °C at a heating rate of 10 °C min^{-1}.

Electrochemical measurements. The electrocatalytic performance of urea synthesis from NO_3^- and CO_2 was evaluated using a CHI 760E electrochemical workstation. A Hg/HgO electrode (filled with 1 M KOH) was used as the reference electrode, while a 1x1 cm^{-2} platinum sheet served as the counter electrode. The working electrode, with a fixed area of 0.25 cm^2, was made of dry carbon fiber paper (CFP) modified with catalysts. For preparation, 10 mg of the catalyst was dispersed in 2 mL of a 1:1 mixture of water and ethanol, followed by the addition of 20 μL of Nafion (5 wt% aqueous solution), then sonicated for 30 minutes to form a homogeneous ink. The CFP was coated with 40 μL of this ink, resulting in a catalyst loading of 0.8 mg cm^{-2}. The working electrodes were vacuum-dried at 60 °C for further use. Prior to electrochemical testing, the cathode chamber of the H-type cell (60 mL) was pre-saturated with the appropriate gas (Ar > 99.999% or CO_2 > 99.999%). During the catalytic process, the gas flow rate was maintained at 30 mL min^{-1}. All potentials were measured against the Hg/HgO reference electrode and converted to the RHE scale using the equation: $E_{RHE} = E_{Hg/HgO} + 0.098 + 0.059 \times pH$. The pH was 6.8 with CO_2 saturation and 8.3 without CO_2 saturation. Linear sweep voltammetry (LSV) tests were conducted at a scan rate of 10 mV s^{-1}. Cyclic voltammetry (CV) curves for electrochemical double-layer capacitance (Cdl) determination were measured within a potential window without Faradic processes, using an electrolyte of 0.1 M $KHCO_3$ and 0.1 M KNO_3 at different scan rates ranging from 20 to 160 mV s^{-1}. Electrochemical impedance spectroscopy (EIS) measurements were carried out at a potential of -0.25 V vs RHE in the frequency range of 0.1 Hz to 10 kHz.

Product detection and efficiency calculation

NO_2^- quantification. Nitrites (NO_2^-) can be diazotized by sulfanilamide in an acid environment, and the resulting diazotized compound can be coupled with N-(1-Naphthyl) ethylenediamine dihydrochloride to produce pink azo dyes that exhibit a characteristic absorption at a wavelength of 540 nm. To prepare the chromogenic reagent, 0.15 g of sulfanilamide was dissolved in 50.0 mL of 2.0 M HCl to create the sulfanilamide solution (Reagent A). Additionally, 20.0 mg of N-(1-Naphthyl) ethylenediamine dihydrochloride was dissolved in 20.0 mL of deionized water to prepare the N-(1-Naphthyl) ethylenediamine dihydrochloride solution (Reagent B). In a typical procedure, 3.0 mL of standard solutions or samples were added to the test tubes, followed by the addition of 200 μL of Reagent A. After mixing and allowing the mixture to stand for 10 minutes, 60 μL of Reagent B was added. The solution was then shaken and left to stand for 30 minutes. The concentration - absorbance curves were calibrated using standard urea solutions, as shown in Figure S5.

NH_4^+ quantification. The NH_4^+ concentration was quantified by indophenol blue method. Typically, a certain amount of electrolyte was taken out from the reaction cell and diluted to 2 mL. Then, 2 mL of 1.0 M NaOH solution containing sodium citrate and salicylic acid and 1 mL of freshly prepared 0.05 M NaClO was added. The mixed solution was shaken for few seconds. Finally, 0.2 mL of 1 wt.% sodium nitroferricyanide solution were added for the colour reaction. After keeping at room temperature for 1 h, the resulting solution was measured using an UV–Vis spectrophotometer The absorbance at ~655 nm was used to determine the concentration of NH_4^+. The concentration - absorbance curves were calibrated using standard urea solutions, as shown in Figure S5.

Urea quantification via diacetyl monoxime (DAMO) spectrophotometry. First, 1 mL of sample solution was removed from the electrochemical reaction vessel. (If a 10-fold dilution is required, take 100 μL of the sample solution and add 900 μL of 0.1 M $KHCO_3$ and 0.1 M KNO_3 electrolyte.). Then 2 mL acid-ferric solution (100ml concentrated phosphoric acid, 300ml concentrated sulfuric acid, 600 mL deionized water and 100mg ferric chloride) and 1 mL diacetyl monoxime (DAMO)-thiosemicarbazide (TSC) solution (5 g DAMO and 100 mg TSC were dissolved in 1,000 mL deionized water) were added. Then the solution was heated to 100 ºC and maintained for 15 min. After cooling to room temperature, the absorbance was acquired at 525 nm using a UV–Vis spectrophotometer (UV-2600). The concentration - absorbance curves were calibrated using standard urea solutions, as shown in Figure S5.

Urea quantification via high-performance liquid chromatography (HPLC). In addition to the DAMO method, high-performance liquid chromatography (HPLC, LC-40D) was employed to detect urea in the product. Chromatographic separation was performed on a 5 μm C18 column with a mobile phase consisting of acetonitrile and water in a 20:80 (v/v) ratio. The flow rate was maintained at 0.2 mL/min, and an injection volume of 20 μL was used. The detection wavelength was set at 195 nm. The Calibration curves were constructed using standard urea solutions, and the concentration-peak integral area was used for quantification, as shown in Figure S6.

Calculations of urea yield rate. The average yield rate of urea was calculated as follow:

$$Y_{urea} = (c_{urea} \times V_{catholyte})/(t \times S)$$

where c_{urea} is the measured urea concentration (μmol mL^{-1}), $V_{catholyte}$ is the total volume of electrolyte (mL), t is time for electrocatalysis and S is the catalyst loading area (cm^2).

Calculations of urea FE. The FE for urea electrosynthesis was calculated as the following equations:

$$FE_{urea} = (16 \times F \times c_{urea} \times V_{catholyte})/Q$$

where F is the Faradaic constant (96485.3 C mol^{-1}) and Q is the total charge passed through the working electrode (C).

Calculations of NO_2^- yield rate. The average yield rate of urea was calculated as follow:

$$Y_{NO_2^-} = (c_{NO_2^-} \times V_{catholyte})/(t \times S)$$

where $c_{NO_2^-}$ is the measured nitrate concentration (μmol mL^{-1}), $V_{catholyte}$ is the total volume of electrolyte (mL), t is time for electrocatalysis and S is the catalyst loading area (cm^2).

Calculations of NO_2^- FE. The FE for urea electrosynthesis was calculated as the following equations:

$$FE_{NO_2^-} = (2 \times F \times c_{NO_2^-} \times V_{catholyte})/Q$$

where F is the Faradaic constant (96485.3 C mol^{-1}) and Q is the total charge passed through the working electrode (C).

Calculations of NH_4^+ yield rate. The average yield rate of urea was calculated as follow:

$$Y_{NH_4^+} = (c_{NH_4^+} \times V_{catholyte})/(t \times S)$$

where $c_{NH_4^+}$ is the measured ammonium concentration (μmol mL^{-1}), $V_{catholyte}$ is the total volume of electrolyte (mL), t is time for electrocatalysis and S is the catalyst loading area (cm^2).

Calculations of NH_4^+ FE. The FE for urea electrosynthesis was calculated as the following equations:

$$FE_{NH_4^+} = (8 \times F \times c_{NH_4^+} \times V_{catholyte})/Q$$

where F is the Faradaic constant (96485.3 C mol^{-1}) and Q is the total charge passed through the working electrode (C).

Quantification of other products via proton nuclear magnetic resonance (^1H NMR). In order to evaluate the presence of possible byproducts generated during the electrocatalytic co-reduction of CO_2 and NO_3^-, ^1H NMR spectroscopy was conducted using a Bruker AVANCE III HD 600 MHz spectrometer with 128 scans averaged per spectrum at 25 ºC. Each sample consisted of 450 μL of the post-electrolysis electrolyte and 50 μL of DMSO-d_6. Standard sample containing 10 mmol L^{-1} of formamide, acetamide, methanol, formic acid, and ethanol were prepared under identical conditions to identify and assign characteristic peaks in the ^1H NMR spectra.

DFT computational details

Density functional theory (DFT) calculations were carried out using the Vienna ab initio simulation package (VASP). The interactions between ions and electrons were modelled using the projector augmented wave (PAW) method, while the Perdew–Burke–Ernzerhof (PBE) functional within the generalized gradient approximation (GGA) was applied. For structural relaxation, a plane wave energy cutoff of 500 eV was selected, and 3×3×1 Monkhorst-Pack k grids were employed for Brillouin zone integrations. The convergence criteria for the iterative process required a maximum residual force of less than 0.02 eV•$Å^{-1}$ and an energy change of less than 10^{-5} eV. A vacuum thickness of 20 Å was used to minimize interlayer interactions. To account for van der Waals interactions, Grimme's DFT-D3 correction method was also included.

The NO_3RR on catalyst surface was simulated according to the following reactions:

$$*NO_3^- + H_2O + e^- \rightarrow *NO_2 + 2OH^-$$

$$*NO_2 + H_2O + 2e^- \rightarrow *NO + 2OH^-$$

$$*NO + H_2O + 2e^- \rightarrow *N + 2OH^-$$

$$*N + H_2O + e^- \rightarrow *NH + OH^-$$

$$*NH + H_2O + e^- \rightarrow *NH_2 + OH^-$$

The CO_2RR on catalyst surface was simulated according to the following reactions:

$$*CO_2 + H^+ + e^- \rightarrow *COOH$$

$$*COOH + H^+ + e^- \rightarrow *CO + H_2O$$

The C-N coupling reactions on catalyst surface was simulated according to the following reactions:

$$*CO + *NH_2 \rightarrow *CONH_2$$

$$*CONH_2 + *NH_2 \rightarrow *CO(NH_2)_2$$

The free energy change (ΔG) of each elementary reaction was calculated as follows:

$$\Delta G = \Delta E + \Delta ZPE - T \times \Delta S$$

where ΔE is the difference of electronic energy between products and reactants, ΔZPE is the change of zero-point energies, and ΔS is the entropy change.

The adsorption energies of intermediates such as *CO, $*NH_2$ and $*NO_3$ were calculated based on the following equation:

$$E_{adsorption} = E_{total} - (E^* + E_{adsorbate})$$

where E_{total}, E^*, and $E_{adsorbate}$ represent the DFT energy of adsorption system, substrate, and adsorbate, respectively.

Additional Figures and Captions

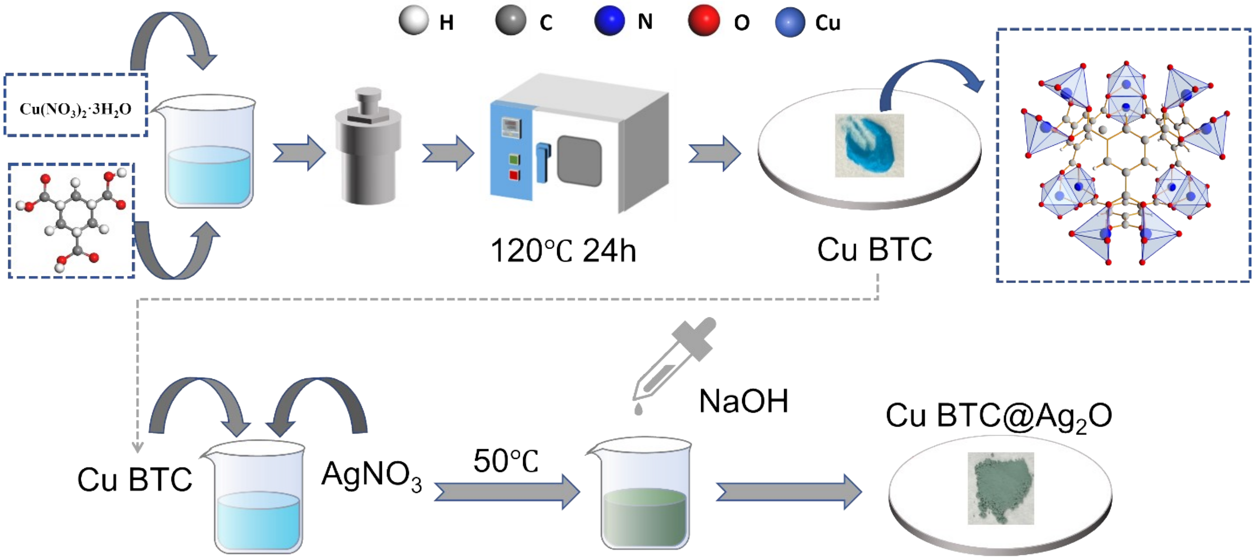

Figure S1. Schematic illustration of the synthesis of Cu BTC@Ag_2O.

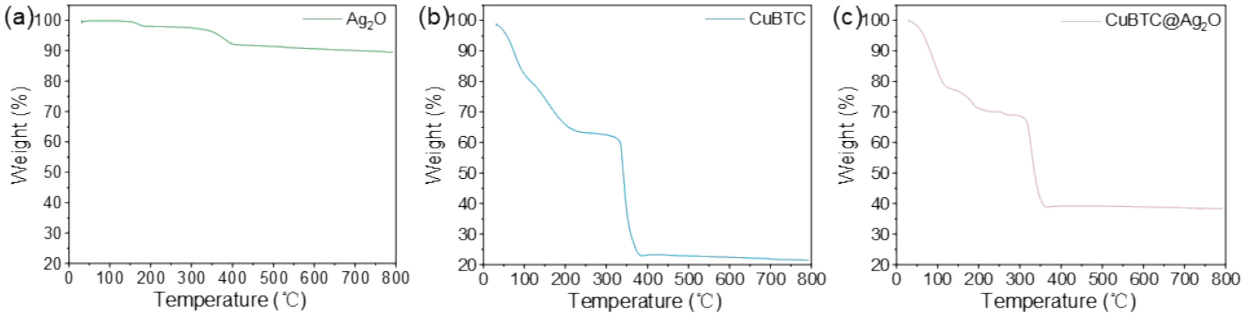

Figure S2. TGA data for (a) Ag_2O; (b) Cu BTC and (c) Cu BTC@Ag_2O.

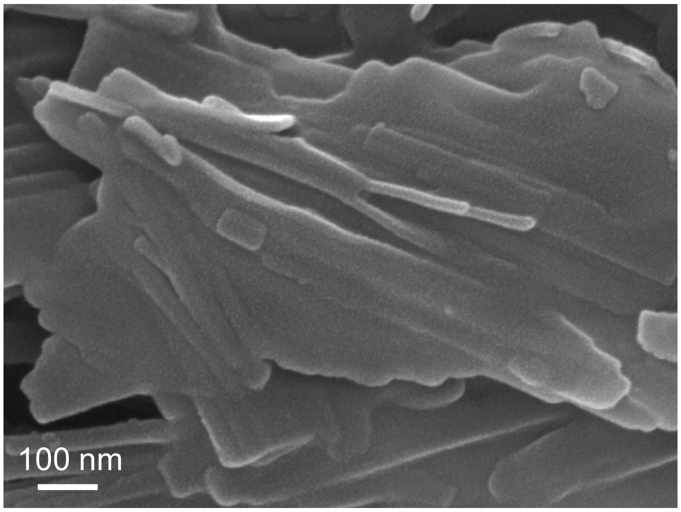

Figure S3. SEM image of Cu BTC@Ag_2O.

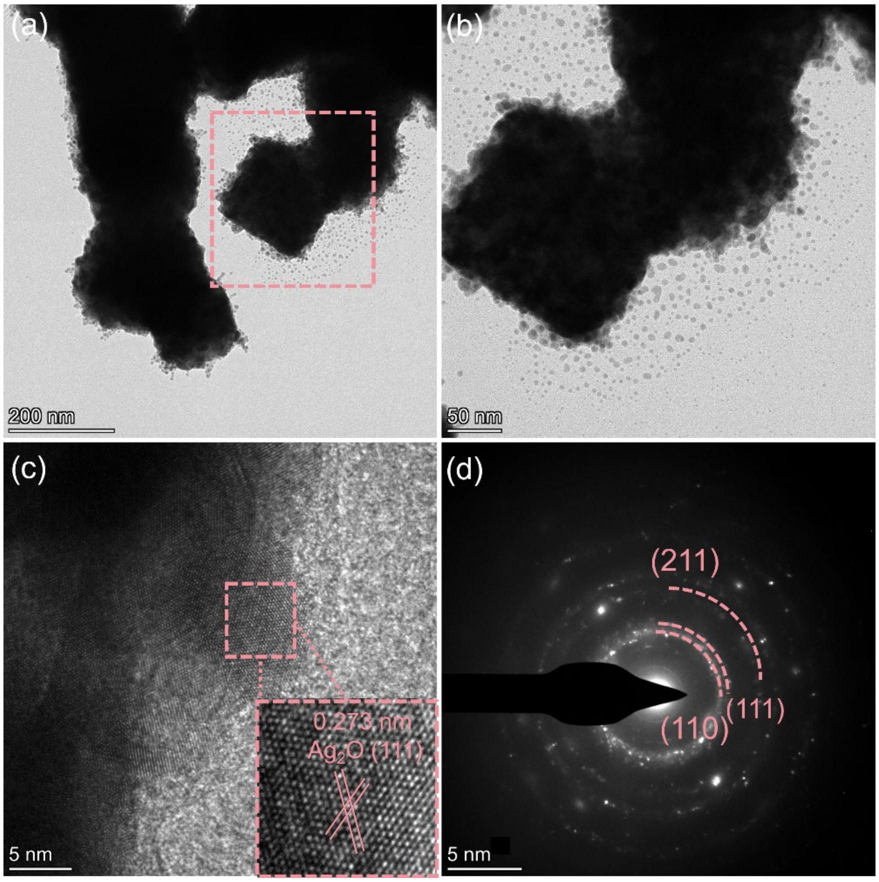

Figure S4. (a) Low magnification TEM image, (b) high magnification TEM image, (c) high-resolution TEM image and (d) SAED of Ag_2O.

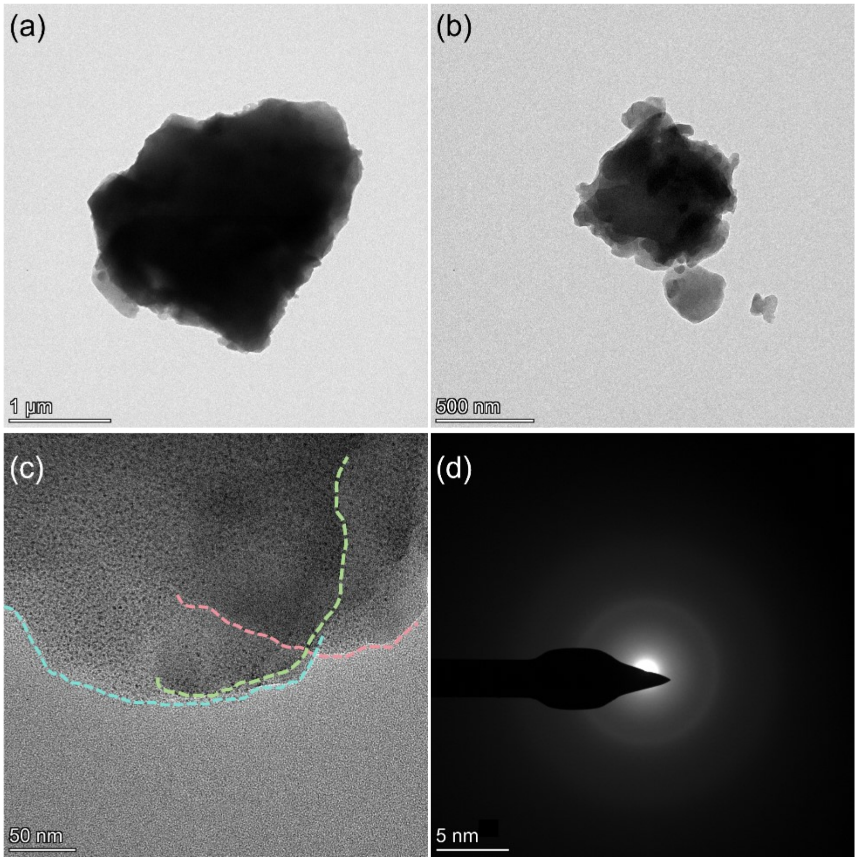

Figure S5. (a) Low magnification TEM image, (b) high magnification TEM image, (c) high-resolution TEM image and (d) SAED of Cu BTC.

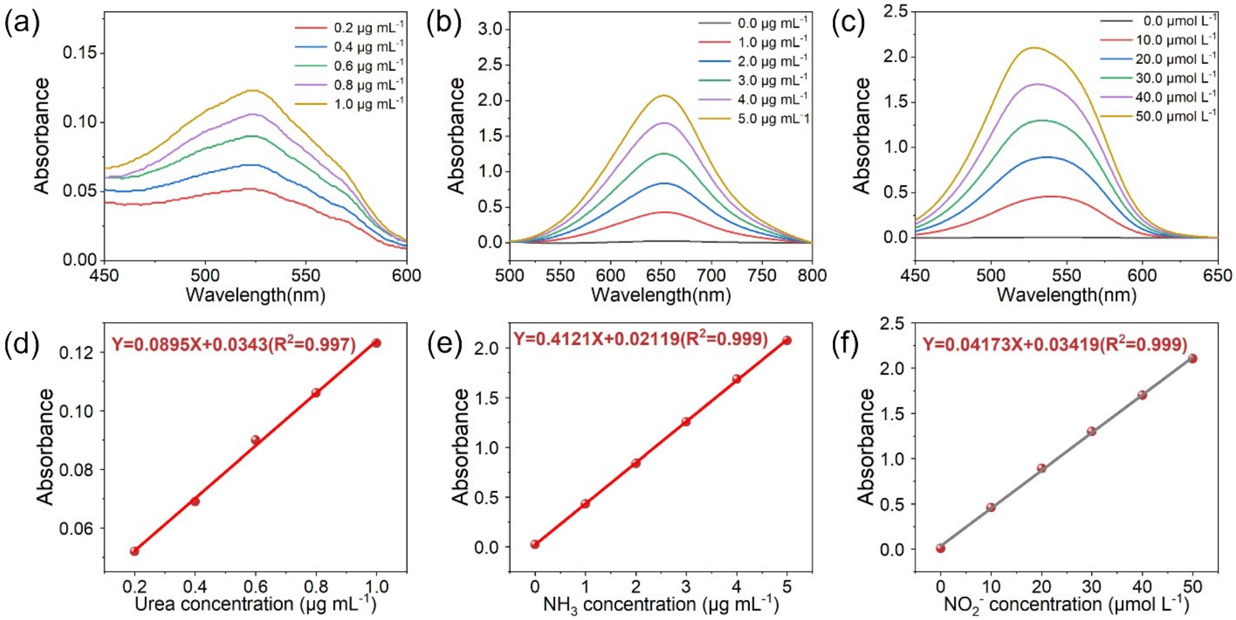

Figure S6. The quantification of urea, NH_4^+ and NO_2^-. (a) UV-vis curves and (d) concentration-absorbance of urea solution with a series of standard concentration (0.0-1.0 μg mL^{-1}) in 0.1M $KHCO_3$ + 0.1M KNO_3. (b) UV-vis curves and (e) concentration-absorbance of NH_4Cl solution with a series of standard concentration (0.0-5.0 μg mL^{-1}) in 0.1M $KHCO_3$ + 0.1M KNO_3. (c) UV-vis curves and (f) concentration-absorbance of KNO_2 solution with a series of standard concentration (0.0-50.0 $\mu molL^{-1}$) in 0.1M $KHCO_3$ + 0.1M KNO_3.

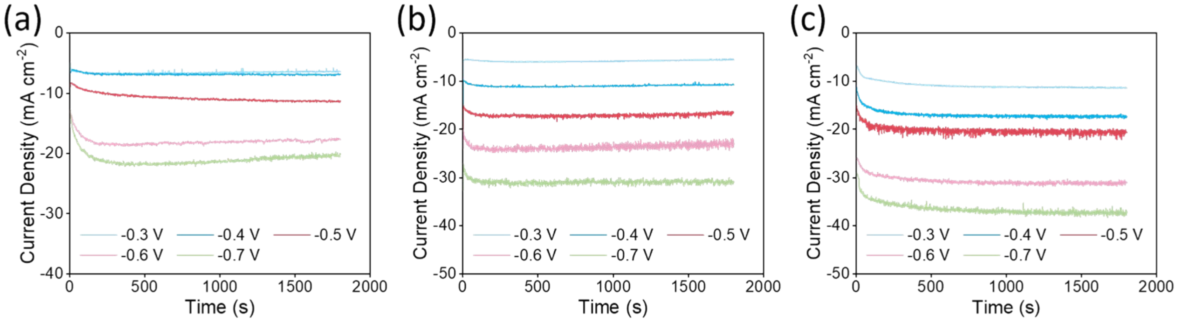

Figure S7. Chronoamperometry curves of (a) Cu BTC, (b) Ag_2O, and (c) Cu BTC@Ag_2O at different potentials for 30 min in CO_2-Saturated 0.1 M $KHCO_3$ with 0.1 M KNO_3 electrolyte.

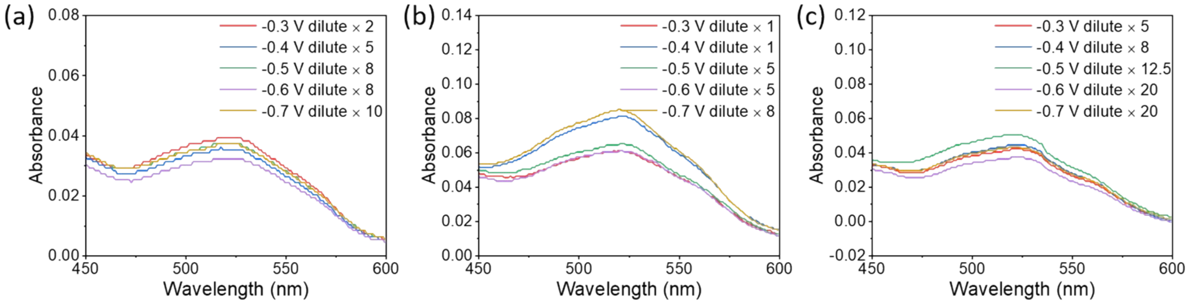

Figure S8. UV−vis absorption spectra of urea assay for (a) Cu BTC, (b) Ag_2O, and (c) Cu BTC@Ag_2O at different potentials. Dilute the electrolyte to a suitable concentration after 30 min of electrolysis.

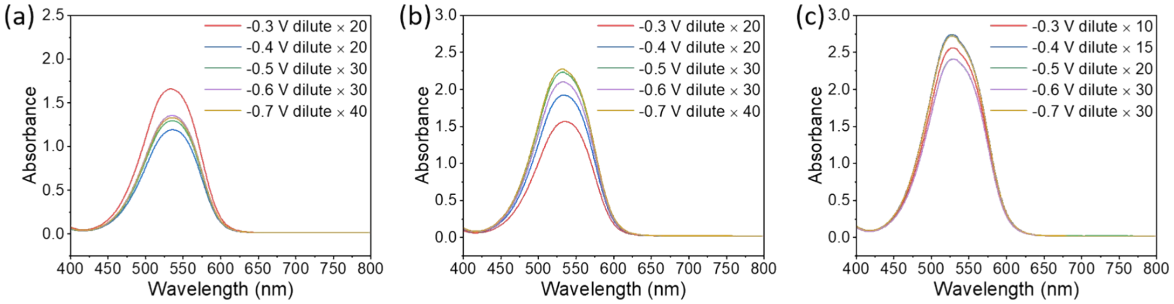

Figure S9. UV−vis absorption spectra of NO_2^- assay for (a) Cu BTC, (b) Ag_2O, and (c) Cu BTC@Ag_2O at different potentials. Dilute the electrolyte to a suitable concentration after 30 min of electrolysis.

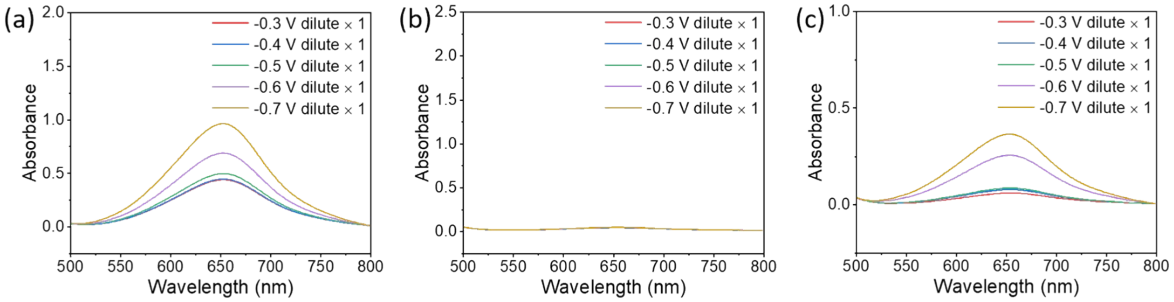

Figure S10. UV−vis absorption spectra of NH_3 assay for (a) Cu BTC, (b) Ag_2O, and (c) Cu BTC@Ag_2O at different potentials. Dilute the electrolyte to a suitable concentration after 30 min of electrolysis.

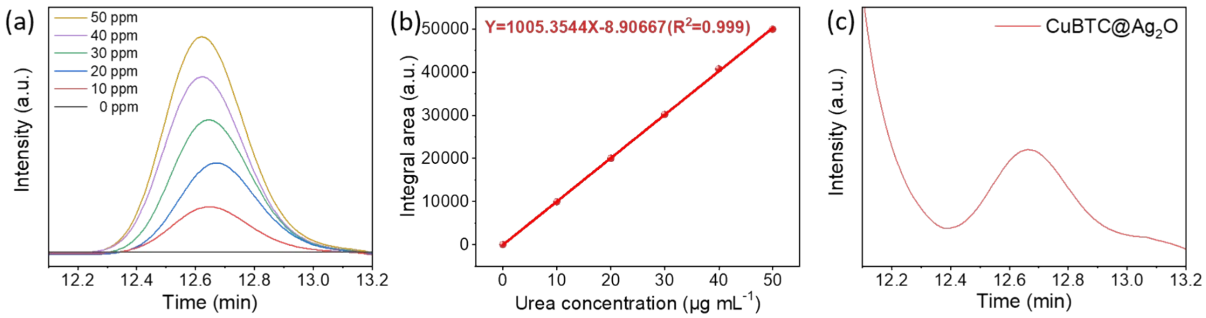

Figure S11. The quantification of urea via high-performance liquid chromatography (HPLC). (a) High-performance liquid chromatogram and (b) corresponding calibration curve for urea solution with a series of standard concentration (0-50 ppm) in 0.1M $KHCO_3$ + 0.1M KNO_3. (c) HPLC measurements of urea from post-electrolysis electrolyte on Cu BTC@Ag_2O catalyst at -0.4 V (vs RHE) for 30 min of electrocatalysis.

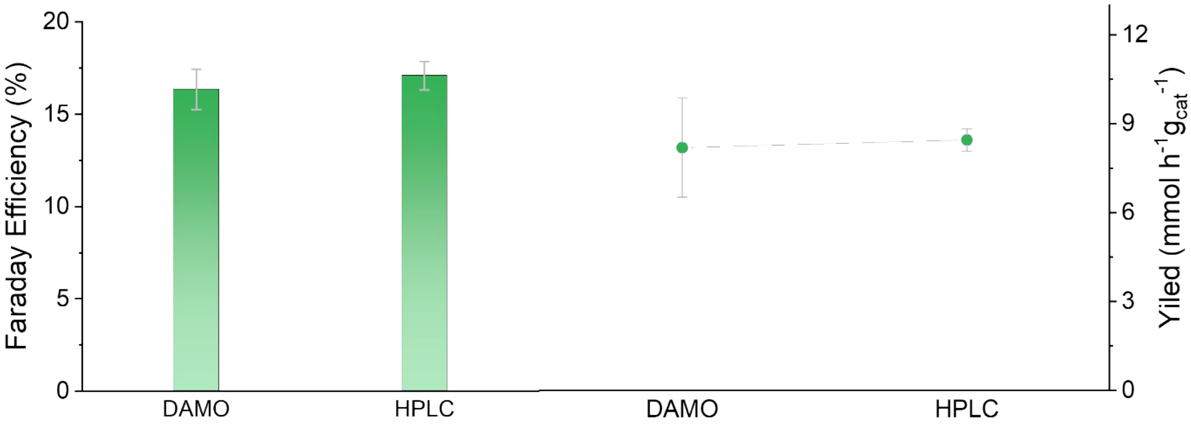

Figure S12. Urea Faraday efficiencies and corresponding yield rates obtained using both DAMO and HPLC methods on Cu BTC@Ag_2O catalyst at -0.4 V (vs RHE) for 30 min of electrocatalysis.

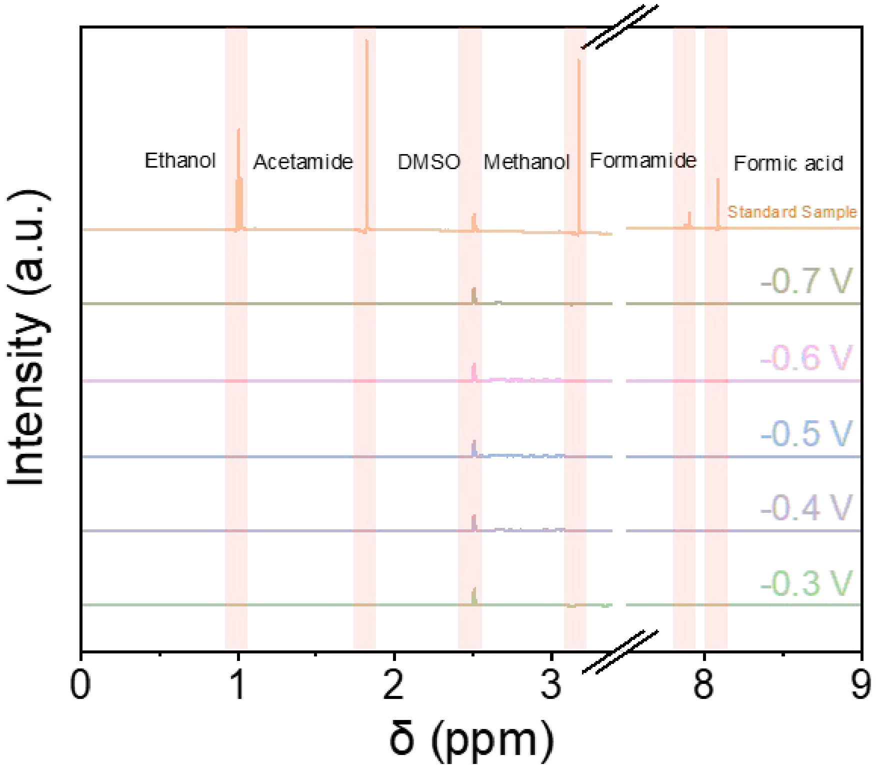

Figure S13. ^{1}H NMR spectra of post-electrolysis electrolyte for Cu BTC@Ag$_2$O catalyst at different potentials after 30 minutes of electrocatalysis with highlighted regions according to common C-N or oxygenated products.

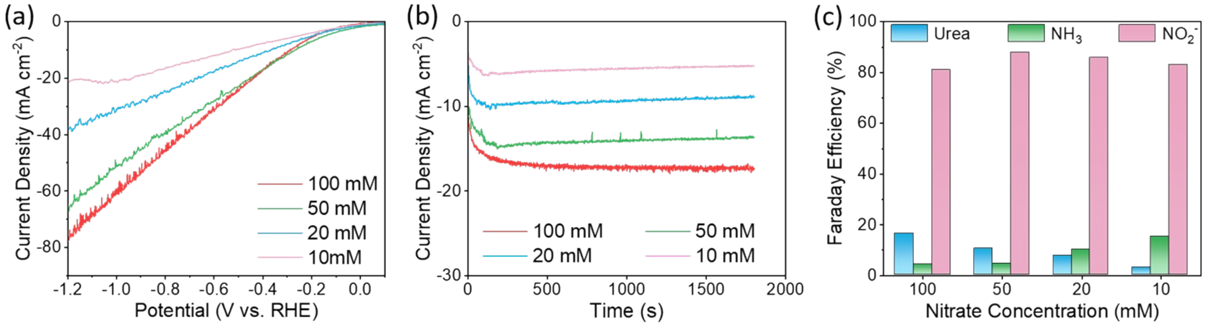

Figure S14. (a) LSV curves of Cu BTC@Ag_2O in different nitrate concentrations (concentrations of 100 mM, 50 mM, 20 mM and 10 mM, respectively) at a scan rate of 10 mV s^{-1}. (b) Chronoamperometry curves of Cu BTC@Ag_2O at different nitrate concentrations for 30 min. (c) Faradaic efficiency of urea, ammonia and nitrite on Cu BTC@Ag_2O at different nitrate concentrations at the potentials of -0.4 V vs. RHE.

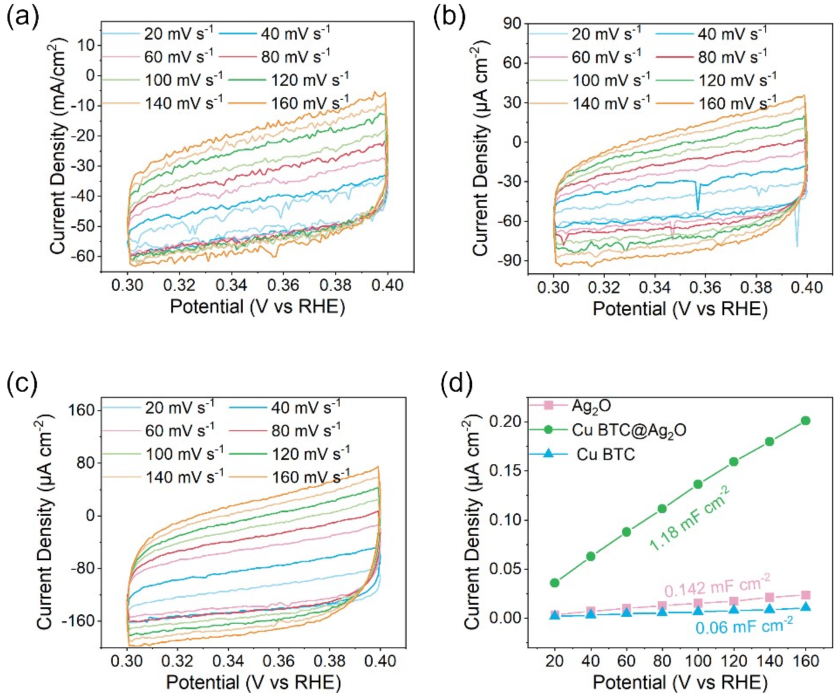

Figure S15. Electrochemically active surface area measurement of different catalysts. The cyclic voltammetry (CV) curves for (a) Cu BTC, (b) Ag_2O and (c) Cu BTC@Ag_2O in the electrolyte of CO_2-saturated 0.1 M $KHCO_3$ with 0.1 M KNO_3. (d) Double layer capacitor of Cu BTC, Ag_2O and Cu BTC@Ag_2O.

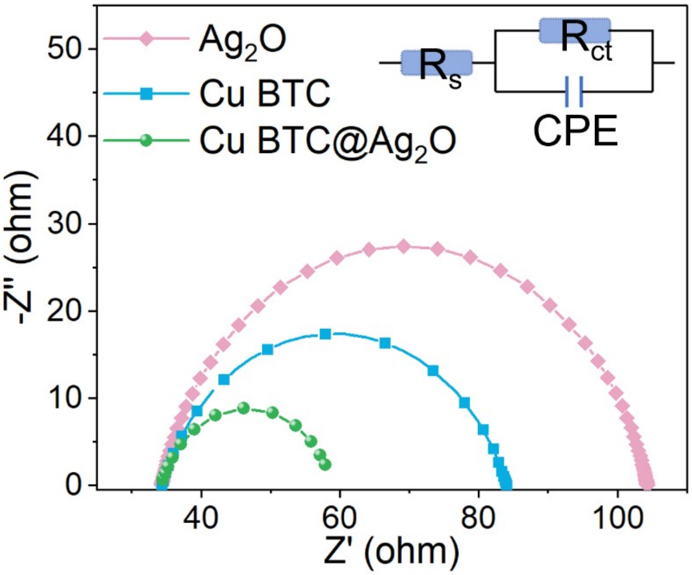

Figure S16. Electrochemical impedance spectroscopy of Cu BTC, Ag$_2$O and Cu BTC@Ag$_2$O in 0.1 M KHCO$_3$ with 0.1 M KNO$_3$ at -0.25 V (vs RHE).

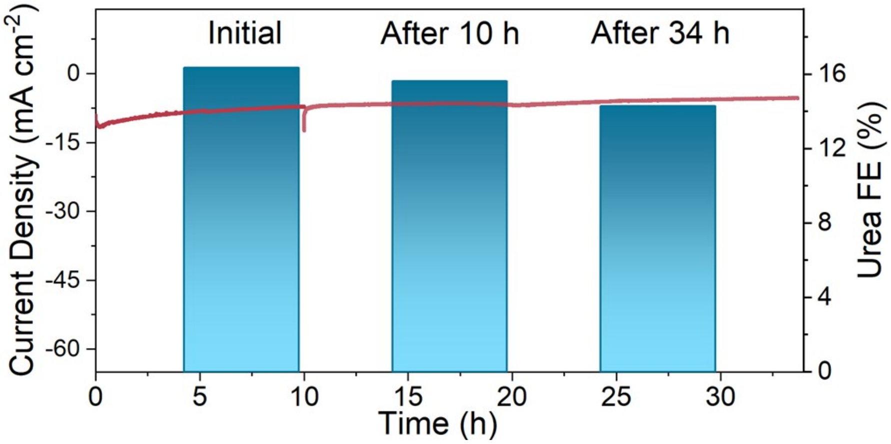

Figure S17. Long-term chronoamperometry tests for Cu BTC@Ag_2O at -0.4 V (vs RHE). The column represents FE of urea measured at different times. The red line represents the current density measured during the test.

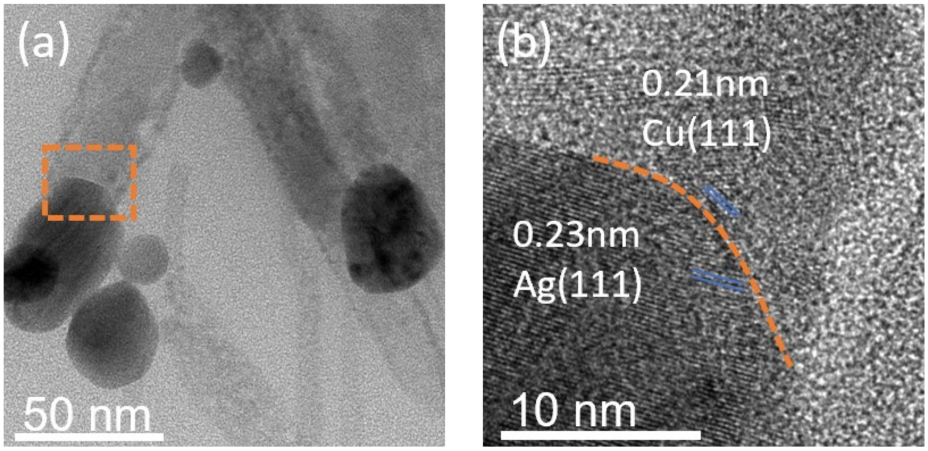

Figure S18. Post-reaction analyses on the Cu BTC@Ag_2O catalyst. (a) TEM image and (b) the corresponding HR-TEM image of Cu BTC@Ag_2O after 30 min of electrocatalysis at -0.4 V.

Table S1. Comparison of the electrocatalytic urea production of Cu BTC@Ag_2O catalyst with other extensively reported electrocatalysis.

Cathode Material	Cell	Maximum FE for urea	Maximum yield for urea (mmol h^{-1} g^{-1})	Potential (V vs RHE)	Electrolyte	Ref.
CuPc-Amino	H-cell	11.9%	103.1	-1.6	0.1M $KHCO_3$ 50mM KNO_3	[1]
Cu_1–CeO_2	H-cell	5.29%	52.84	-1.6	0.1M $KHCO_3$ 50mM KNO_3	[2]
Vo-enriched CeO_2	H-cell	3.8%	15.71	−1.6	0.1M $KHCO_3$ 50mM KNO_3	[3]
Cu-Cu_2O	H-cell	17.72%	62.4	-1.5	0.1M $KHCO_3$ 50mM $NaNO_3$	[4]
Electron-deficient Cu	H-cell	14.3%	255.0	-1.4	0.1M $KHCO_3$ 0.1M KNO_3	[5]
Cu@Zn	H-cell	9.28%	7.9	-1.02	0.2M $KHCO_3$ 0.1M KNO_3	[6]
AuCuIrCo MEI	H-cell	22.57%	52.43	-0.9	0.02M KNO_3	[7]
$BiVO_4$@MIL	H-cell	23.5%	47.7	-0.9	0.1M KNO_3	[8]
TiO_2-C	Flow cell	48.9%	43.37	-0.9	0.1M KNO_3	[9]
$FeNi_3$ alloy	H-cell	16.58%	8.27	-0.9	0.1M KNO_3	[10]
Cu_8Ni_2/C	H-cell	25.1%	37.53	−0.5/−0.8	0.1M $KHCO_3$ 0.1M KNO_3	[11]

CuAu SAA	H-cell	45.2%	13.56	-0.74	0.1M KNO_3	[12]
$SrRuO_3$	H-cell	34.1%	25.34	-0.7	0.1M KNO_3	[13]
Cu_2O	H-cell	16.84%	22.89	-0.6	0.1M $KHCO_3$ 10mM KNO_3	[14]
F-Cu	H-cell	24.9%	17.33	-0.6	0.1M $KHCO_3$ 0.1M KNO_3	[15]
α-CuZn	H-cell	21.4%	29.3	-0.52	0.05M KNO_3	[16]
Vo-InOOH	H-cell	51%	9.87	-0.5	0.1M KNO_3	[17]
a-$Cu_{0.1}CoB_x$	H-cell	27.7%	5.19	-0.5	0.1M KNO_3	[18]
AuPd	H-cell	15.6%	3.37	-0.5	0.1M $KHCO_3$ 10mM KNO_3	[19]
Mo–PdIn BNRs	H-cell	18.42%	16.92	-0.4	0.1M KNO_3	[20]
Ru-Cu CF	H-cell	25.4%	2.52	-0.3	0.1M $NaNO_3$	[21]
$CuWO_4$	H-cell	70.1%	1.64	-0.2	0.1 M KNO_3	[22]
Cu BTC@Ag_2O	H-cell	16.4%	11.2	-0.4/-0.5	0.1M $KHCO_3$ 0.1M KNO_3	This work

Table S2. Adsorption configuration of $^*CO_2$, $^*COOH$, $^*CO$ on Ag, Cu, and Cu-Ag surfaces.

	Ag	Cu	Cu-Ag
$^*CO_2$	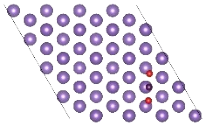	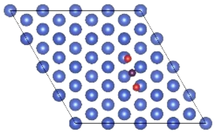	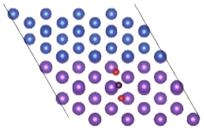
$^*COOH$	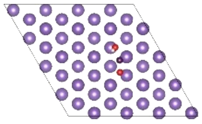	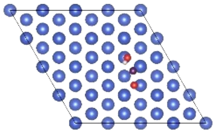	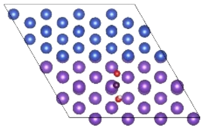
$^*CO$	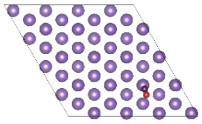	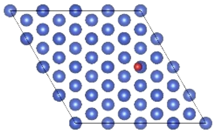	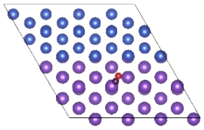

Table S3. Adsorption configuration of *NO_3, *NO_2, *NO, *N, *NH, *NH_2 on Ag, Cu, and Cu-Ag surfaces.

	Ag	Cu	Cu -Ag
*NO_3	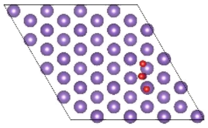	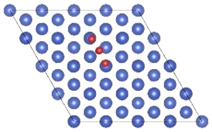	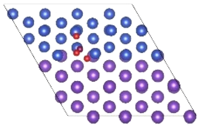
*NO_2	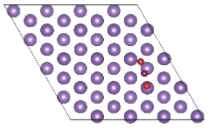	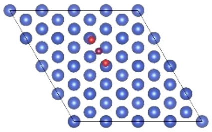	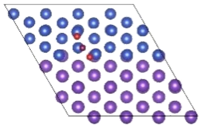
*NO	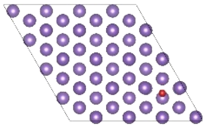	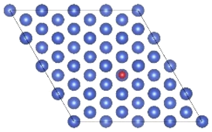	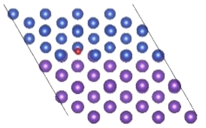
*N	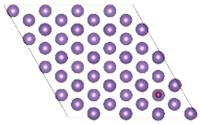	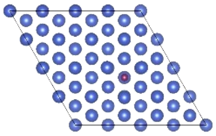	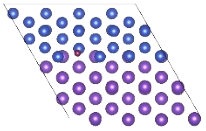

*NH	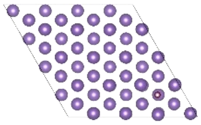	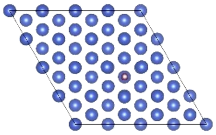	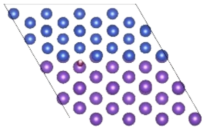
*NH_2	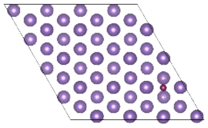	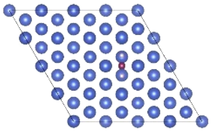	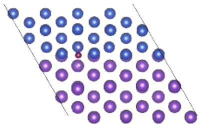

Table S4. Adsorption configuration of intermediates for C-N coupling on Ag, Cu, and Cu-Ag surfaces.

	Ag	Cu	Cu-Ag
*CO+*NH$_2$	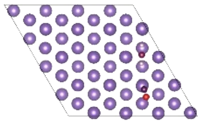	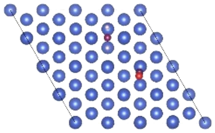	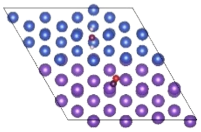
*CONH$_2$	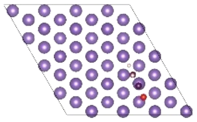	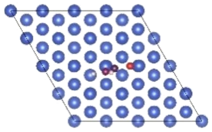	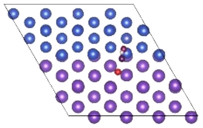
*CONH$_2$+*NH$_2$	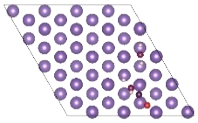	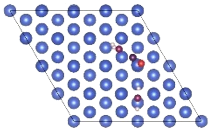	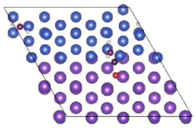
*CO (NH$_2$)$_2$	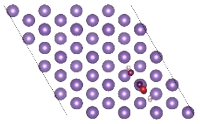	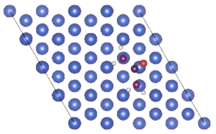	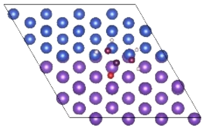

References

[1] H. Li, L. Xu, S. Bo, Y. Wang, H. Xu, C. Chen, R. Miao, D. Chen, K. Zhang, Q. Liu, Ligand engineering towards electrocatalytic urea synthesis on a molecular catalyst, Nat. Commun., 15 (2024) 8858.
[2] X. Wei, Y. Liu, X. Zhu, S. Bo, L. Xiao, C. Chen, T.T.T. Nga, Y. He, M. Qiu, C. Xie, Dynamic reconstitution between copper single atoms and clusters for electrocatalytic urea synthesis, Adv. Mater., 35 (2023) 2300020.
[3] X. Wei, X. Wen, Y. Liu, C. Chen, C. Xie, D. Wang, M. Qiu, N. He, P. Zhou, W. Chen, Oxygen vacancy-mediated selective C–N coupling toward electrocatalytic urea synthesis, J. Am. Chem. Soc., 144 (2022) 11530-11535.
[4] J. Zhao, Y. Yuan, F. Zhao, W. Han, Q. Yuan, M. Kou, J. Zhao, C. Chen, S. Wang, Identifying the facet-dependent active sites of Cu2O for selective CN coupling toward electrocatalytic urea synthesis, Appl. Catal. B, 340 (2024) 123265.
[5] Y. Wang, X. Zhu, Q. An, X. Zhang, X. Wei, C. Chen, H. Li, D. Chen, Y. Zhou, Q. Liu, Electron Deficiency is More Important than Conductivity in C− N Coupling for Electrocatalytic Urea Synthesis, Angew. Chem., 136 (2024) e202410938.
[6] N. Meng, X. Ma, C. Wang, Y. Wang, R. Yang, J. Shao, Y. Huang, Y. Xu, B. Zhang, Y. Yu, Oxide-derived core–shell Cu@ Zn nanowires for urea electrosynthesis from carbon dioxide and nitrate in water, ACS Nano., 16 (2022) 9095-9104.
[7] X. Chen, Y. Tan, J. Yuan, S. Zhai, L. Su, Y. Mou, W.Q. Deng, H. Wu, Enhancing Urea Electrosynthesis From CO2 and Nitrate Through High‐Entropy Alloying, Advanced Energy Materials, (2025) 2500872.
[8] S. Yao, S.Y. Jiang, B.F. Wang, H.Q. Yin, X.Y. Xiang, Z. Tang, C.H. An, T.B. Lu, Z.M. Zhang, Polyoxometalate confined synthesis of BiVO4 nanocluster for urea production with remarkable O2/N2 tolerance, Angew. Chem., 137 (2025) e202418637.
[9] X. Huang, Y. Li, S. Xie, Q. Zhao, B. Zhang, Z. Zhang, H. Sheng, J. Zhao, The tandem nitrate and CO2 reduction for urea electrosynthesis: role of surface N‐intermediates in CO2 capture and activation, Angew. Chem., Int. Ed., 63 (2024) e202403980.
[10] T. Hou, J. Ding, H. Zhang, S. Chen, Q. Liu, J. Luo, X. Liu, FeNi 3 nanoparticles for electrocatalytic synthesis of urea from carbon dioxide and nitrate, Materials Chemistry Frontiers, 7 (2023) 4952-4960.
[11] Y. Zhou, B. Yang, Z. Huang, G. Chen, J. Tang, M. Liu, X. Liu, R. Ma, Z. Mei, N. Zhang, Cu-Ni alloy nanocrystals with heterogenous active sites for efficient urea synthesis, Appl. Catal. B, 343 (2024) 123577.
[12] P. Zhan, J. Zhuang, S. Yang, X. Li, X. Chen, T. Wen, L. Lu, P. Qin, B. Han, Efficient electrosynthesis of urea over single‐atom alloy with electronic metal support interaction, Angew. Chem., Int. Ed., 63 (2024) e202409019.
[13] L. Lv, H. Tan, Y. Kong, B. Tang, Q. Ji, Y. Liu, C. Wang, Z. Zhuang, H. Wang, M. Ge, Breaking the scaling relationship in C− N coupling via the doping effects for efficient urea electrosynthesis, Angew. Chem., Int. Ed., 63 (2024) e202401943.
[14] S. Chen, G. Hai, H. Cheng, D. Xie, G.F. Chen, L.X. Ding, H. Wang, Efficient urea electrosynthesis via coordination of the reaction rate of carbon dioxide and nitrate co‐reduction, AIChE Journal, 70 (2024) e18515.

[15] J. Lin, L. Duan, J. Zhang, X. Quan, R. Du, G. Chen, X. Liu, R. Ma, N. Zhang, Halogen-interacted copper with surface reconstructed charge distributions for efficient urea production, Applied Catalysis B: Environment and Energy, 371 (2025) 125268.

[16] S. Zhai, Z. Peng, X. Chen, Y. Tan, Y.-F. Huang, Z. Liu, W.-Q. Deng, H. Wu, Brass Phase Determining Selectivity in Urea Electrosynthesis from CO2 and Nitrate, ACS Catal., 15 (2025) 3276-3283.

[17] C. Lv, C. Lee, L. Zhong, H. Liu, J. Liu, L. Yang, C. Yan, W. Yu, H.H. Hng, Z. Qi, A defect engineered electrocatalyst that promotes high-efficiency urea synthesis under ambient conditions, ACS Nano., 16 (2022) 8213-8222.

[18] Y. Wu, H. Lin, Q. Mao, H. Yu, K. Deng, J. Wang, L. Wang, Z. Wang, H. Wang, Trace Cu - Induced Low C— N Coupling Barrier on Amorphous Co Metallene Boride for Boosting Electrochemical Urea Production, Small., 20 (2024) 2407679.

[19] H. Wang, Y. Jiang, S. Li, F. Gou, X. Liu, Y. Jiang, W. Luo, W. Shen, R. He, M. Li, Realizing efficient CN coupling via electrochemical co-reduction of CO2 and NO3-on AuPd nanoalloy to form urea: Key CN coupling intermediates, Appl. Catal. B, 318 (2022) 121819.

[20] Y. Xu, S. Wang, Y. Wu, Q. Mao, H. Yu, K. Deng, Z. Wang, L. Wang, H. Wang, Alloying effect modulated electronic structure of Mo-doped PdIn bimetallene nanoribbons for ambient electrosynthesis of urea, Chem. Commun., 61 (2025) 2317-2320.

[21] J. Qin, N. Liu, L. Chen, K. Wu, Q. Zhao, B. Liu, Z. Ye, Selective electrochemical urea synthesis from nitrate and CO2 using in situ Ru anchoring onto a three-dimensional copper electrode, ACS Sustain. Chem. Eng., 10 (2022) 15869-15875.

[22] Y. Zhao, Y. Ding, W. Li, C. Liu, Y. Li, Z. Zhao, Y. Shan, F. Li, L. Sun, F. Li, Efficient urea electrosynthesis from carbon dioxide and nitrate via alternating Cu–W bimetallic C–N coupling sites, Nat. Commun., 14 (2023) 4491.